View metadata, citation and similar papers at core.ac.uk

brought to you by CORE

provided by CiteSeerX

Constitutive Laws for Biomechanical Modeling of Refractive Surgery

Michael R. Bryant

Peter J. McDonnell

Doheny Eye Institute and Department of Ophthalmology,
University of Southern California School of Medicine,
Los Angeles, CA 90033

Membrane inflation tests were performed on fresh, intact human corneas using a fiber optic displacement probe to measure the apical displacements. Finite element models of each test were used to identify the material properties for four different constitutive laws commonly used to model corneal refractive surgery. Finite element models of radial keratotomy using the different best-fit constitutive laws were then compared. The results suggest that the nonlinearity in the response of the cornea is material rather than geometric, and that material nonlinearity is important for modeling refractive surgery. It was also found that linear transverse isotropy is incapable of representing the anisotropy that has been experimentally measured by others, and that a hyperelastic law is not suitable for modeling the stiffening response of the cornea.

Introduction

Keratorefractive surgical procedures are designed to increase or decrease the radius of curvature of the cornea and thereby reduce or eliminate refractive errors in the eye. In radial keratotomy, for example, the surgeon makes a radial pattern of incisions in the cornea. The incisions weaken the peripheral cornea, which bows outward in response to the internal pressure in the eye, thereby flattening the central cornea. Although technically simple, this procedure has resulted in 30 percent of patients being undercorrected by more than one diopter, and 10 percent of patients being overcorrected by more than one diopter (Waring et al., 1987).

Finite element-based biomechanical models of the eye have been presented in recent years as tools to help better predict radial keratotomy and other refractive surgeries. For the most part, these models have been based on standard constitutive laws with material properties either culled from the literature or chosen to give reasonable results. Hanna et al. (1988), Vito et al. (1989) and Bryant et al. (1987) have presented models of refractive surgery employing linear elastic isotropy. Recognizing the layered structure of the corneal stroma, with its inherent anisotropy, Hanna et al. (1989a) and Bryant and Velinsky (1991) employed transversely isotropic constitutive laws to model arcuate and radial incisions and radial keratotomy, respectively. Modeling the cornea as an elastomer, Hanna et al. (1989b) applied the Mooney-Rivlin law in a biomechanical model of radial keratotomy. The constants for a materially nonlinear isotropic law were identified by Wray et al. (1994) by comparing their model to previously reported pressure-volume data and to clinical results from two studies of radial keratotomy.

Huang et al. (1988) established the first constitutive law formulated specifically for radial keratotomy by defining an effective corneal thickness based on a qualitative description of the distribution of cut fibrils in the corneal stroma resulting from a pattern of radial keratotomy incisions. Pinsky and Datye (1991) took this approach a step further by mathematically deriving the distribution of cut fibrils from an assumed arrangement of corneal lamellae, and used this to define an effective stiffness for a thin shell model of radial keratotomy. They have recently extended this approach to a fully three-dimensional finite element formulation that includes interlamellar shear effects, making this the first general, geometrically nonlinear finite element formulation that represents the cornea's lamellar microstructure in detail (Pinsky and Datye, 1994).

Because of the difficulty of performing good, controlled experiments of radial keratotomy and other refractive surgeries, none of these models have been accurately verified against the results of refractive surgery. Consequently, it is not known if one of the more common constitutive laws, such as transverse isotropy or the Mooney-Rivlin law, is adequate to model keratorefractive surgery, or if a more complex formulation, such as Pinsky and Datye's, is required. Similarly, it is not known which features (e.g., nonlinearity or anisotropy) are most important in modeling refractive surgery or how the different formulations vary in predicting the results of radial keratotomy. This study sought to answer some of these questions by performing side-by-side comparisons of different constitutive laws that are readily available and commonly used to model radial keratotomy. To enable the comparison, the material constants for the different laws were identified from the same experimental data, which were generated from membrane inflation tests on fresh, human corneas.

Materials and Methods

1 Experimental Measurements. Fresh human corneas were obtained from the Lions Doheny Eye Bank (an affiliate of Tissue Banks International). The corneas had been preserved in corneal storage medium (Optisol GS, Chiron, Irvine, CA) at 4°C within 24 hours of patient death. All corneas were used within eight days of preservation. The corneas retained a 2–3 mm scleral rim, but all other ocular structures (iris, ciliary body, etc.) had been removed. Testing was conducted at room temperature (21°C) with the corneas covered in a bath of 15 percent dextran (295,000 MW, Sigma Co., St. Louis, MO), a high molecular weight substance that has been demonstrated to maintain corneal thickness within the physiological range (Duffey et al., 1989). To bring a cornea into equilibrium with the test conditions, it was submersed in the dextran solution for approximately 30 minutes prior to testing. The cornea was then mounted on an artificial anterior chamber (custom design, Lions Doheny Eye Bank), shown in Fig. 1, which clamped against the scleral rim, allowing the cornea to maintain its natural curvature.

The epithelium was mechanically removed from the cornea with a blunt instrument, and the central corneal thickness was

Contributed by the Bioengineering Division for publication in the JOURNAL OF BIOMECHANICAL ENGINEERING. Manuscript received by the Bioengineering Division March 30, 1994; revised manuscript received September 23, 1995. Associate Technical Editor: R. P. Vito.

Copyright © 1996 by ASME

Downloaded From: https://biomechanical.asmedigitalcollection.asme.org on 06/28/2019 Terms of Use: http://www.asme.org/about-asme/terms-of-use

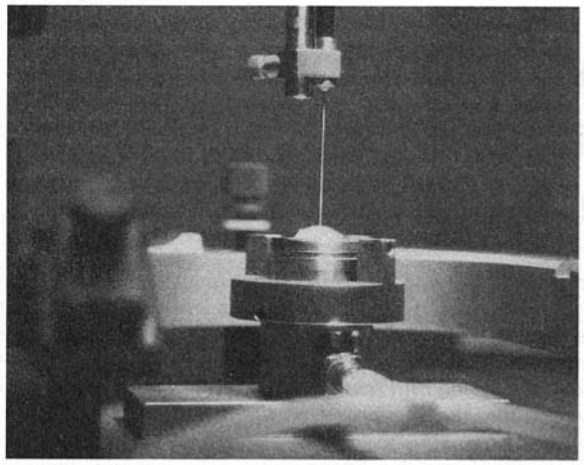

Fig. 1 Artificial anterior chamber, shown mounted with human cornea and with fiber optic displacement probe positioned over corneal apex. The water bath, normally mounted on the top surface of the chamber and surrounding the cornea, has been removed.

then measured to the nearest micron with an ultrasonic pachymeter (DGH 1000, DGH Technology, Inc., Frazer, PA). Digital calipers were used to measure the corneal diameter at the longest meridian and at the meridian perpendicular to that, and the two values were averaged to obtain a mean corneal diameter. A drop of silver paint, approximately 2 mm in diameter, was placed on the corneal apex to serve as a target for the fiber optic probe. The paint was allowed to dry 5 minutes before submerging the cornea in the dextran bath. To pressurize the cornea, a bottle of 15 percent dextran was connected to the artificial anterior chamber and to a digital pressure gauge. The pressure gauge had an accuracy of approximately 1 mm Hg with a precision of 0.1 mm Hg. The pressure was adjusted by changing the vertical position of the bottle.

A fiber optic displacement probe (Model 88N1, Philtec, Arnold, MD) was used to record the apical displacement of the cornea after each pressure change. The probe had a resolution of less than 1 μm and was calibrated at the factory. Based on our ability to set and maintain the gain required to match the calibration curve, we estimated the accuracy of the probe to be about 3 μm.

Before testing a cornea, it was preconditioned by cycling it between the pressures of 40 mm Hg and less than 1 mm Hg. Three complete cycles were performed, holding the pressure approximately 10 minutes at the extremes of each cycle. The pressure gauge and the fiber optic probe were then reset, and the test was started. Beginning at a low pressure of less than 1 mm Hg, the pressure in the artificial anterior chamber was incrementally increased in ten steps: 0.5, 2, 4, 6, 10, 14, 19, 24, 30, and 40 mm Hg. The pressure sequence was then reversed. So that the data would represent the cornea's steady-state response, the tissue was allowed to creep after each pressure change before the probe output was recorded. Readings were taken when the probe output was stable to 0.01 V, corresponding to approximately 1.4 μm, for at least 2 minutes. This resulted in times between pressure changes of about 10–20 minutes.

After the test was completed, the probe output was checked at both the high (40 mm Hg) and low (less than 1 mm Hg) pressures to determine the extent of drift in the probe output. The apical height (in the sagittal direction) of the specimen was then measured at the lowest pressure (less than 1 mm Hg) with the digital calipers. To determine if the corneal thickness had remained stable throughout the test, the pachymetry measurement was repeated.

Since the probe output gives relative rather than absolute displacement, the origin of the pressure-displacement curve was located by linearly extrapolating from the two lowest measurement points (at 0.5 and 2 mm Hg).

2 Identification of Material Properties Using Finite Element Analysis. Finite element analysis was performed using COSMOS/M (Structural Research and Analysis Corp., Santa Monica, CA) on a 486 PC. The corneas were modeled as axisymmetric structures, with the axis of symmetry along the anterior-posterior axis of the eye (Fig. 2). The radial distance, R in Fig. 2, was set to one half the average diameter, as determined from the measurements described above. The height of the corneal apex in the sagittal direction, H, and the corneal thickness at the apex, T_a, were set to the measured values. The peripheral thickness, T_p, was set to 0.65 mm. Each model consisted of 150 four-node isoparametric axisymmetric (two-dimensional) elements and 186 nodes (Fig. 2), resulting in 354 equations. The corneal material was assumed to be homogeneous, and the small scleral rim where the cornea was clamped was not modeled. The symmetry condition at the corneal apex was imposed by constraining nodes along the y (anterior-posterior) axis against displacement in the x (radial) direction, and nodes along the peripheral edge of the model were fixed, representing clamping of the artificial anterior chamber against the scleral rim. A uniform pressure distribution was applied normal to the posterior surface of the model.

Individual finite element models were constructed for each measured cornea. Four different constitutive laws were considered: linear elastic isotropy, nonlinear elastic isotropy, linear transverse isotropy, and hyperelasticity (Ogden's model). In addition, geometric nonlinearity was added to a second set of linear isotropic models. In each case, the material parameters (Young's modulus, nonlinear modulus, or Ogden's coefficients) were chosen to match the measured pressure-displacement curve to the one generated by the finite element model. Although some hysteresis was evident in all samples, the material properties were chosen to match only the pressure-displacement curve for increasing loading.

Linear Elastic Isotropy. For the linear isotropic models, a tangent modulus was calculated at 15 mm Hg, a value that is close to the mean for a normal population (Hart, 1992). The objective was to generate a load-displacement curve tangent to the measured curve at 15 mm Hg (0.002 N/mm^2) (Fig. 3). To correspond to the measured data, the displacement for the finite element generated pressure-displacement curves was defined as the y (sagittal) displacement of the node at the apex on the anterior surface of the model. Since the linear finite element solution takes a different path than the measured displacement, the finite element model had to start at a different unloaded geometry in order to intersect the nonlinear curve at 15 mm Hg. This difference in geometry is shown as ΔH in Fig. 3.

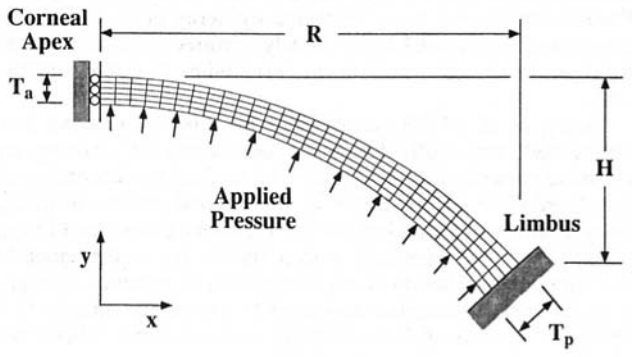

Fig. 2 Axisymmetric finite element mesh used to model the membrane inflation experiments. The anterior and posterior surfaces follow concentric circular arcs defined by the radial size of the cornea, R, the apical height of the cornea, H, and the corneal thicknesses at the apex, T_a, and periphery (limbus), T_p.

Downloaded From: https://biomechanical.asmedigitalcollection.asme.org on 06/28/2019 Terms of Use: http://www.asme.org/about-asme/terms-of-use

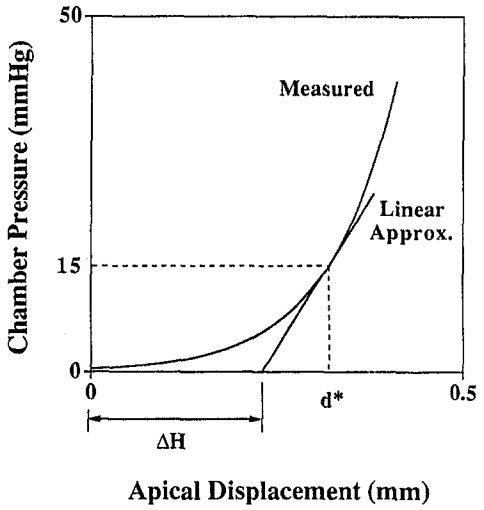

Fig. 3 Method for determining the tangent modulus for the materially linear constitutive laws. The modulus for the linear model is chosen so that at 15 mm Hg, the linear model's pressure-displacement curve intersects the measured curve at that pressure.

Accordingly, the value of H, as in Fig. 2, for the linear model was set to $H_m + \Delta H$, where H_m was the measured value of the apical height of the cornea.

Models were constructed with and without geometric nonlinearity. For the former, a total Lagrangian formulation with a Newton-Raphson solution method was used. Poisson's ratio, ν, was set to 0.49 in all cases. The modulus, E, was chosen so that the calculated pressure-displacement curve intersected the measured one at 15 mm Hg, i.e., so that the displacement at 15 mm Hg was equal to $d^* - \Delta H$, where d^* was the measured displacement at 15 mm Hg (Fig. 3). With geometric nonlinearity, convergence was achieved by varying the modulus according to a simple, linear scaling law:

$$E_{i+1} = E_i^* D_i / D_{i+1} \tag{1}$$

where i represents the current solution step, $i + 1$ the next step, and D the apical displacement in the y direction, so that D_{i+1} is the target displacement, $d^* - \Delta H$. Convergence to within 1 μm on displacement was typically achieved in less than six steps.

Linear Elastic Transverse Isotropy. A common form of anisotropy is transverse isotropy, in which there is material symmetry about an axis, so that the material behaves isotropically in planes normal to that axis. Taking the z axis, normal to the corneal surface, as the axis of symmetry, with x and y parallel to the corneal lamellae, the stress-strain (material property) matrix for transverse isotropy can be written as follows (Boresi and Chong, 1987):

$$E = \begin{pmatrix} E_{11} & E_{12} & E_{13} & & & \\ & E_{11} & E_{13} & & 0 & \\ & & E_{33} & & & \\ & & & E_{44} & & \\ & \text{Symmetric} & & & E_{55} & \\ & & & & & E_{55} \end{pmatrix} \tag{2}$$

where

$$E_{11} = E_p(1 - \nu_{xz}^2/n)/C$$

$$E_{12} = E_p(\nu_{xy} + \nu_{xz}^2/n)/C$$

$$E_{13} = E_p\nu_{xz}(1 + \nu_{xy})/(nC)$$

$$E_{33} = E_p(1 - \nu_{xy}^2)/(nC)$$

$$E_{44} = (E_{11} - E_{12})/2$$

$$E_{55} = G_{xz}$$

and $C = 1 - \nu_{xy}^2 - 2\nu_{xz}^2/n - 2\nu_{xy}\nu_{xz}^2/n$. E_p is the modulus of elasticity in the in-plane (x and y) directions, ν_{ij} is the Poisson's ratio in the ij plane, relating strain applied in the i direction to the resulting strain in the j direction, G_{xz} is the shear modulus in the xz and yz planes, $n = E_p/E_z$, and E_z is the modulus of elasticity in the transverse direction (normal to the corneal surface).

The transversely isotropic finite element models were defined with the following values for these constants:

$$n = 10$$

$$\nu_{xy} = \nu_{xz} = 0.5 \tag{3}$$

and

$$G_{xz} = \frac{E_p}{1 + n(1 + 2\nu_{xz})}.$$

The constant n, relating the moduli in the in-plane and transverse directions, was chosen based on the work of Battaglioli and Kamm (1984), who measured the transverse modulus for the sclera and found it to be at least one order of magnitude lower than reported values of the in-plane modulus.

As with the isotropic models, the in-plane modulus, E_p, was chosen so that the finite element pressure-displacement curve was tangent to the measured curve at 15 mm Hg. The same identification scheme as described above for isotropy was employed here. All transversely isotropic models included geometric nonlinearity.

Nonlinear Isotropy. Material nonlinearity was modeled with a nonlinear stress-strain relationship that is similar to the one employed by Woo et al. (1972) and used more recently by Wray et al. (1994):

$$\sigma = \alpha(e^{\beta\epsilon_{ef}} - 1) \tag{4}$$

in which ϵ_{ef} is effective strain, and α and β are the material constants.

Effective strain is defined by COSMOS/M according to an equivalence between the strain energy density expressed in terms of effective stress and effective strain and the strain energy density expressed in terms of the individual components of stress and strain. For the general 3-D case, the effective strain can be expressed as (Chang, 1994)

$$\epsilon_{ef} = \left[\frac{1 - \nu}{(1 + \nu)(1 - 2\nu)} (\epsilon_{xx}^2 + \epsilon_{yy}^2 + \epsilon_{zz}^2) + \frac{2\nu}{(1 + \nu)(1 - 2\nu)} (\epsilon_{xx}\epsilon_{yy} + \epsilon_{yy}\epsilon_{zz} + \epsilon_{xx}\epsilon_{zz}) + \frac{1}{2(1 + \nu)} (\gamma_{xy}^2 + \gamma_{yz}^2 + \gamma_{zx}^2) \right]^{1/2} \tag{5}$$

Downloaded From: https://biomechanical.asmedigitalcollection.asme.org on 06/28/2019 Terms of Use: http://www.asme.org/about-asme/terms-of-use

where ν is Poisson's ratio, and γ_{ij} are components of the engineering shear strain.

In the finite element solution, equilibrium is satisfied incrementally (see, for example, Cook, 1981), and the element stiffness matrices are based on the tangent modulus, E, that is calculated for the current values of effective strain.

The material constants α and β were chosen to match the finite element generated pressure-displacement curve as closely as possible to the measured curve, which was accomplished by solving the following least-squares optimization problem:

$$\min_{\mathbf{x}} \tfrac{1}{2} \| \mathbf{f}(\mathbf{x}) \|_2^2 \tag{6}$$

where

$$\mathbf{f}(\mathbf{x}) = (d_1 - d_1^m, d_2 - d_2^m, \ldots, d_{np} - d_{np}^m)^T,$$

d_i is the calculated displacement at the ith pressure, d_i^m is the measured displacement at the ith pressure, np is the number of points along the pressure-displacement curve at which displacements are recorded, and $\mathbf{x} = (\alpha, \beta)^T$.

The optimization process was carried out with a quasi-Newton algorithm using BFGS updates (Gill et al., 1981). To enable convergence, α and β were scaled at each iteration by the average of the values from the current and previous steps. The jacobian matrix, $\partial \mathbf{f}_i / \partial \mathbf{x}_j$, was approximated using backward differences. The process was halted when α and β had converged to within 3 significant figures, which typically required 10–20 iterations.

Hyperelasticity. Hyperelastic constitutive laws, such as the Mooney-Rivlin law, are commonly used to model elastomers (e.g., rubber and rubber-like materials). Another, somewhat more general hyperelastic formulation is Ogden's law, which, for a first-order model, is defined by a strain-energy density function of the form:

$$W = \frac{\mu}{\gamma} (\lambda_1^\gamma + \lambda_2^\gamma + \lambda_3^\gamma - 3) \tag{7}$$

where the λ_i's are the principal stretch ratios and μ and γ are the material constants (COSMOS/M Advanced Modules User Guide, 1993). As with the Mooney-Rivlin law, Ogden's law is an inherently isotropic formulation.

Trial and error was used to find values for γ and μ such that the finite element response matched the measured pressure-displacement curve. Specifically, values of γ from -1000 to 10 were tried, where, for each one, the value of μ was varied until the endpoint of the calculated curve (the displacement at 40 mm Hg) matched the measured curve.

3 Modeling Radial Keratotomy. To compare the capabilities of the different constitutive laws, a four-incision radial keratotomy was modeled for a representative cornea as if it were clamped on the artificial anterior chamber. The finite element mesh was based on the same cross-sectional model geometry depicted in Fig. 2, with the parameter values listed in Table 1. Material properties were based on the average properties identified from the membrane inflation tests and listed in Table 2. Because a four-incision surgery was modeled, a three-dimensional finite element model with quarter symmetry was employed. Eight-node isoparametric (brick) elements were used, and the incisions were represented by relaxing the boundary conditions of nodes along the two incision surfaces, as has been done in previous models of radial keratotomy (Bryant and Velinsky, 1991). The model consisted of 960 elements and 1305 nodes, with four elements through the thickness. The preoperative state was obtained from a model without incisions but otherwise identical to the incised model. The following constitutive laws were compared: linear isotropic with geometric nonlinearity, linear transversely isotropic with geometric nonlinearity, and nonlinear isotropic.

The objective was to determine the average corneal curvature change and its standard deviation based on the material properties identified from the membrane inflation experiments. For the linear isotropic and transversely isotropic laws, results were generated at plus and minus one standard deviation of the average (tangent) moduli measured for the respective constitutive laws. Because the tangent moduli were used in these models, the value of H was set to $H_m + \Delta H_{\text{ave}}$, where ΔH_{ave} is the average value of ΔH, calculated over all measured corneas; H_m was chosen as shown in Table 1 (1.07 mm) to give a reasonable preoperative curvature for the materially nonlinear models.

The corneal curvature change, k, was calculated by subtracting the curvature of the model with no incisions from the curvature of the model with incisions and was calculated at two different meridians: along one incision (0 deg), and between two incisions (45 deg). The curvature (in diopters) was calculated according to $337.5/r$, where r (mm) is the radius of the circle fit to the apical node and the node 1.5 mm from the apex on the anterior surface. This is based on an effective index of refraction for the cornea (1.3375) and approximates the way in which clinical keratometers measure curvature for the central 3 mm of the cornea. The standard deviation of the corneal curvature change, k, for the materially nonlinear isotropic law was calculated in terms of the variances of the parameters α and β by forming a first order Taylor expansion of $k(\alpha, \beta)$ about the average values of α and β.

The mean corneal curvature changes for the three constitutive laws were compared using two-tailed t tests in which a P-value of 0.05 or less was considered statistically significant.

Results

1 Experimental Measurements. Twelve corneas (ages 20–69) were successfully tested. The probe output remained reasonably steady during each test, drifting by no more than about 10 percent. The corneal thickness also remained stable, typically measuring 401–404 μm both before and after each test. Typical measured pressure-displacement curves are shown in Fig. 4. In Fig. 4(a) the results for cornea #2 are shown, including the curves for both the increasing and decreasing loadings. The considerable nonlinearity in the response suggests a stiffening effect with increasing load. The hysteresis revealed in this figure was evident in all the samples; however, we did not quantify it. The increasing loading portion of the response is shown for five representative corneas in Fig. 4b. Interestingly, in each case the knee of the curve occurs around normal intraocular pressure (approximately 12–20 mm Hg).

2 Finite Element Identification. The identification results are summarized in Table 2. There was no significant difference between the in-plane modulus of elasticity for transverse

Table 1 Parameters for the three-dimensional finite element models of radial keratotomy constructed using the geometric model depicted in Fig. 2. Models were constructed assuming linear elastic isotropy, linear elastic transverse isotropy, and materially nonlinear isotropy.

Parameter	Value
Corneal radius, R	5.725 mm
Thickness at apex, T_a	0.482 mm
Thickness at limbus, T_p	0.65 mm
Height at apex,	
H_m	1.07 mm (materially nonlinear law)
$H_m + \Delta H_{\text{ave}}$	1.32 mm (linear isotropic and anisotropic laws)
Number of incisions	4
Clear zone size	4 mm
Incision depth	74%
Intraocular pressure	15 mm Hg (0.002 N/mm^2)

Downloaded From: https://biomechanical.asmedigitalcollection.asme.org on 06/28/2019 Terms of Use: http://www.asme.org/about-asme/terms-of-use

Table 2 Material properties for twelve human corneas, obtained by applying a finite element identification approach to the results of membrane inflation experiments. The first three columns contain the elastic modulus; the last two columns contain the constants for the materially nonlinear law shown in (4)

Cornea	Isotropic, geometric nonlinearity, E (N/mm^2)	Isotropic, linear, E (N/mm^2)	Transversely isotropic, E (N/mm^2)	Isotropic, material nonlinearity, α (N/mm^2)	Isotropic, material nonlinearity, β
1	0.762	0.806	0.763	16.0×10^{-4}	43.0
2	0.592	0.634	0.594	5.20×10^{-4}	42.6
3	0.785	0.837	0.787	8.77×10^{-4}	54.0
4	0.592	0.637	0.592	5.71×10^{-4}	43.2
5	0.674	0.727	0.672	15.0×10^{-4}	36.7
6	0.711	0.743	0.715	14.0×10^{-4}	40.0
7	0.954	1.02	0.955	37.0×10^{-4}	43.5
8	1.37	1.40	1.38	13.3×10^{-4}	85.7
9	0.939	0.982	0.939	23.8×10^{-4}	73.5
10	0.650	0.683	0.652	40.5×10^{-4}	34.7
11	0.630	0.652	0.635	14.2×10^{-4}	41.3
12	0.763	0.815	0.764	16.5×10^{-4}	41.3
Average	0.79	0.83	0.79	17.5×10^{-4}	48.3
Std. dev.	0.22	0.22	0.22	11.1×10^{-4}	15.6

isotropy and the modulus of elasticity for linear elastic isotropy (both including geometric nonlinearity). However, the modulus for isotropic linear elasticity without geometric nonlinearity was six percent larger than when geometric nonlinearity was included.

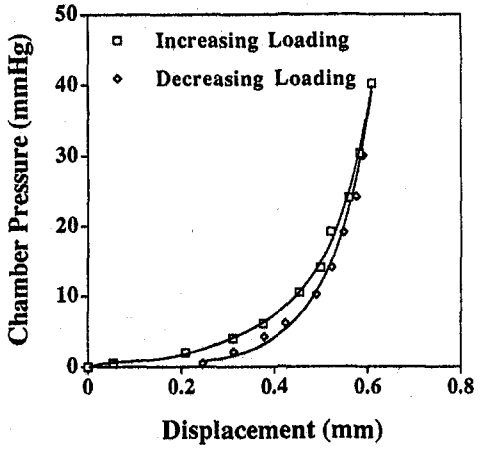

Fig. 4(*a*)

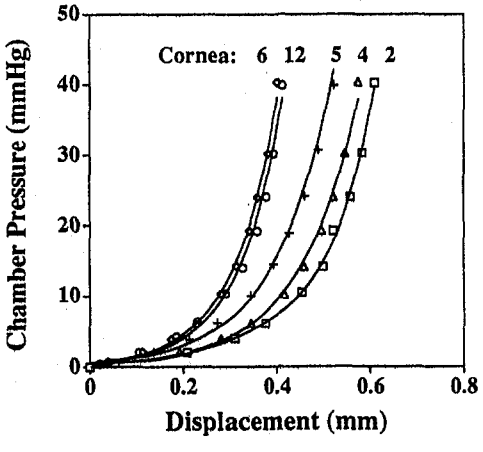

Fig. 4(*b*)

Fig. 4 Measured pressure-displacement curves. (*a*) Results for cornea #2, demonstrating the hysteresis that was evident in all samples. (*b*) Increasing loading curves for five different samples: cornea #'s 2, 4, 5, 6, and 12.

In Fig. 5 the finite element pressure-displacement curves for linear elastic isotropy with and without geometric nonlinearity are shown for cornea #3. As intended, they are tangent to the measured curve at 15 mm Hg and are very similar, demonstrating how little the inclusion of geometric nonlinearity contributes to the nonlinearity of the cornea's response to increasing pressure. The pressure-displacement curves resulting from the transversely isotropic models were almost identical to those of the linear isotropic models.

Typical nonlinear isotropic model results are shown in Fig. 6. The stress-strain curve for cornea #11 (Fig. 6(a)) resulting from the minimization problem (6) has a shape that is very similar to the measured pressure-displacement curve, shown in Fig. 6(b). The finite element generated pressure-displacement curve calculated using the stress-strain curve of Fig. 6(a) fits the measured curve very closely, as shown in Fig. 6b.

Ogden's model provided a very poor fit to the data over the range of values that were attempted (Fig. 7). As shown in Fig. 7 for cornea #1, the stiffening effect of the corneal response to increasing pressure was not well represented by this model over a range of γ from -1000 to 10 (μ from -4.1×10^{-5} N/mm^2 to 0.048 N/mm^2). Values of γ equal to -10^4 and -10^5 were attempted to improve the fit, but the finite element solution failed to converge for these values. Since such a poor fit was

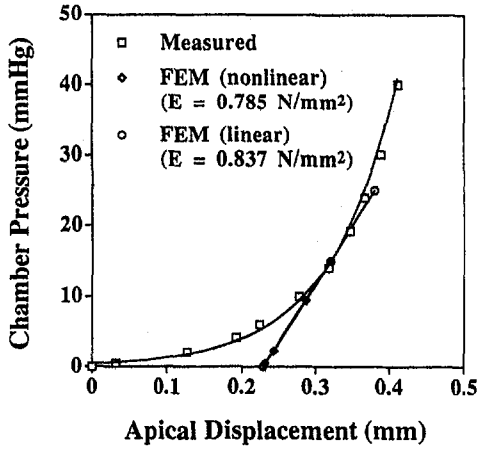

Fig. 5 Finite element identification results for the linear elastic isotropic models with and without geometric nonlinearity for cornea #3, shown tangent to the measured curve at 15 mm Hg

Downloaded From: https://biomechanical.asmedigitalcollection.asme.org on 06/28/2019 Terms of Use: http://www.asme.org/about-asme/terms-of-use

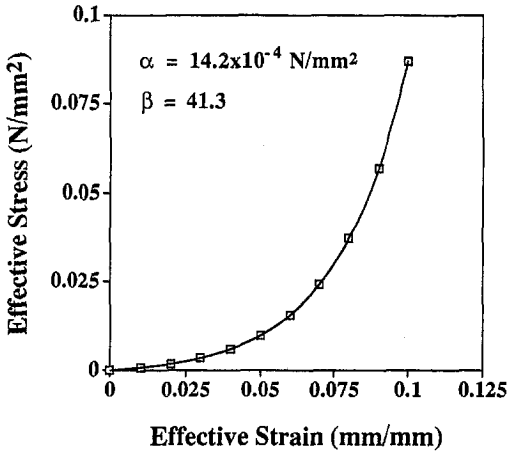

Fig. 6(*a*)

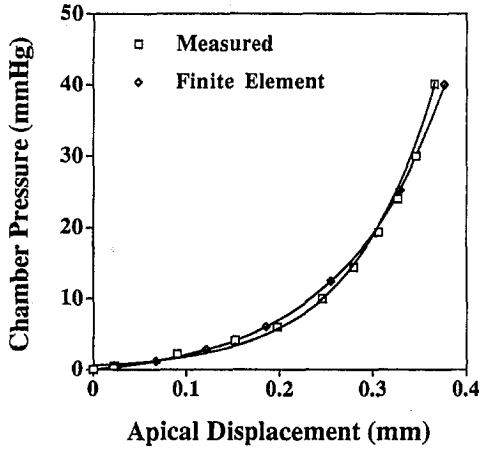

Fig. 6(*b*)

Fig. 6 Finite element identification results for the materially nonlinear isotropic model for cornea #11. (*a*) Exponential stress-strain curve (4) identified from the measured pressure-displacement curve according to (7). Stress and strain are effective values, based on (6). (*b*) Calculated pressure-displacement curve, based on the stress-strain curve shown in (*a*).

obtained for cornea #1, we did not attempt to fit this model to any other data.

3 Radial Keratotomy. The finite element results for the models of radial keratotomy are summarized in Fig. 8. As shown in the figure, more curvature change resulted from assuming a nonlinear modulus than from employing either the linear isotropic or transversely isotropic constitutive laws. This difference was statistically significant in both cases and at both 0 deg (along an incision) and 45 deg (between two incisions); $P < 0.001$ in all cases. The results of the transversely isotropic model were not significantly different from those of the linear isotropic model at either 0 deg ($P = 0.09$) or 45 deg ($P = 0.38$). Slightly more astigmatism—the difference between the curvature changes at 0 deg and 45 deg—was predicted by the transversely isotropic model, although this difference was not statistically significant.

To illustrate the effect of material nonlinearity, the stresses at key points in the cornea were followed from before surgery to afterwards. Shown plotted on the stress-strain curve, these points indicate how much the modulus of elasticity changes during surgery (Fig. 9). In Fig. 9(*a*), points a and b are near an incision; point a is near the anterior corner of the incision at the edge of the clear zone, while point b lies underneath point a, at the posterior cornea of the incision. At point a, the modulus

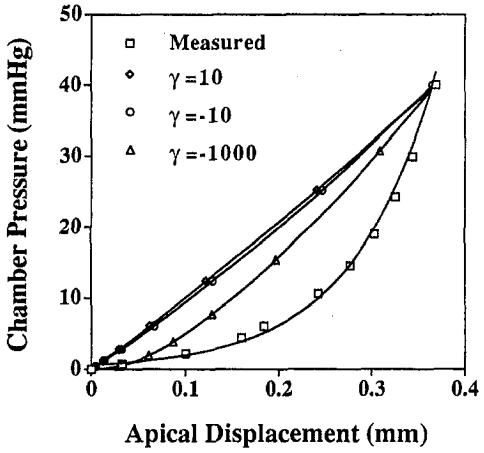

Fig. 7 Results of fitting Ogden's model (8) to the measured pressure-displacement results for cornea #1

increases from 1.32 to 2.33 N/mm² (76 percent increase) during surgery; while at point b, the modulus increases from 0.42 to 0.75 N/mm² (80 percent increase). Two points that lie away from the incision are shown in Fig. 9(*b*). Point *c* is just inside the clear zone, at 45 deg to either adjacent incision, and point d is along the same meridian but outside the clear zone. At both of these points, the effective stress and the modulus decrease during surgery. The modulus decreases from 1.32 to 1.18 N/mm² (10 percent decrease) at point c, and from 0.27 to 0.24 N/mm² (10 percent decrease) at point d.

Discussion

The material properties of the cornea are usually measured either by tensile testing or membrane inflation. The problems associated with tensile testing strips of cornea have been well documented (e.g., Hoeltzel et al., 1992) and include adequately securing the tissue to the clamps, straightening an initially curved strip, accurately measuring the cross-sectional area of the strip, as well as the problem of basing a three-dimensional model of an anisotropic material on the results of a uniaxial tensile test. We chose to test intact corneas to avoid these problems. Woo et al. (1972), in the most complete study of intact corneas, used a "flying spot scanner" to measure the horizontal displacement at the apex, but this required them to paint the entire cornea with ink and place two strips of tape on the cornea as targets for the scanner. More recent studies have employed

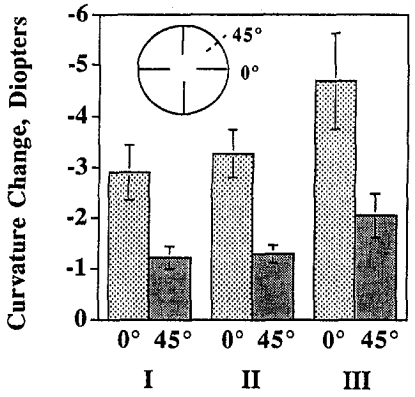

Fig. 8 Corneal curvature change after radial keratotomy for three different constitutive laws: I—linear elastic isotropy with geometric nonlinearity, II—linear elastic transverse isotropy with geometric nonlinearity, and III—materially nonlinear elastic isotropy. A four incision surgery with a 4 mm clear zone was modeled; curvature changes were computed along the incisions (0 deg) and between adjacent incisions (45 deg)

Downloaded From: https://biomechanical.asmedigitalcollection.asme.org on 06/28/2019 Terms of Use: http://www.asme.org/about-asme/terms-of-use

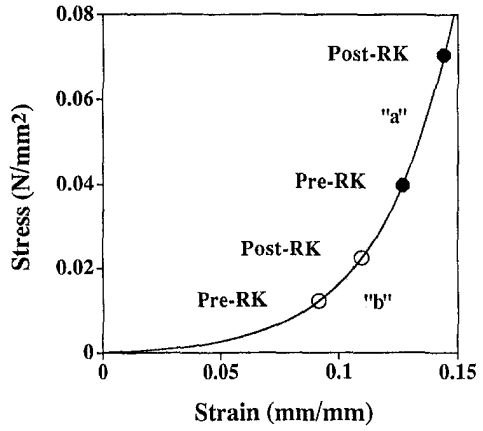

Fig. 9(*a*)

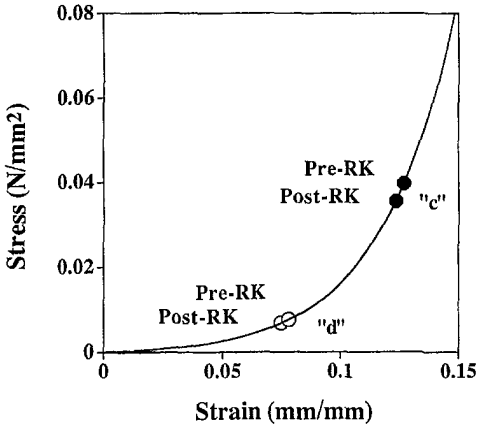

Fig. 9(*b*)

Fig. 9 Stress-strain curves during radial keratotomy (RK) surgery showing how the stress at different points changes from before surgery (Pre-RK) to immediately after surgery (Post-RK). (*a*) Points a and b lie near the central edge of an incision. (*b*) Points c and d lie at 45 deg to adjacent incisions, inside and outside the clear zone, respectively.

better methods of measuring the corneal displacements (Jue and Maurice, 1986; Hjortdal and Koch-Jensen, 1992) without emphasizing the identification of material properties.

Our experimental setup provided us with a number of advantages over other methods. The fiber optic probe enabled noncontact measurement of the cornea, submicron resolution, and the use of a fluid bath, which stabilized the cornea's hydration. This gave us time to let the cornea creep at each load step while it reached most of its steady-state response. Consequently, the estimated material properties represent the steady-state behavior of the tissue. Because the artificial anterior chamber required only a small scleral rim for attachment, the chamber was effective in isolating the cornea for measurement purposes and simplified the specification of boundary conditions in the finite element model.

The most significant problem with our setup was maintaining a flat, mirror-like surface for the probe. The drop of silver paint that we applied for this purpose was highly reflective, nearly flat, and because of its small size (approximately 1–2 mm) and its complete lack of penetration into the cornea, probably had a negligible effect on the cornea's response. However, it was clear that in some cases the paint spot did not remain entirely flat, which may be the source of the 10 percent drift in probe output measured during the test. Another source of error may be the cornea thickness, which we consistently measured to be about 20 percent lower than the normal (in vivo) thickness. This was probably from using a dextran solution with an inappropriately high concentration and may have resulted in an overestimation of the elastic modulus.

The identification process was intended to provide a baseline set of corneal material properties for some of the most common constitutive laws in a way that would enable comparisons between the different laws. Probable sources of error in the estimation process include the simplifications of the assumed geometry and the assumption of homogeneity of the cornea. In particular, the assumption of material homogeneity implies that the identified properties are average properties for the cornea. Nonetheless, because these assumptions were maintained for each constitutive law, they should not affect the comparisons that were made among the radial keratotomy results.

In previous efforts to estimate Young's modulus for the cornea using intact specimens, values have ranged from 0.025 N/mm^2 (Sjontoft and Edmund, 1987) to 17 N/mm^2 (Hjortdal and Koch-Jensen, 1992) at measurement pressures of 10 mm Hg and 100 mm Hg, respectively. It is apparent that the identified modulus depends on the applied pressure, as suggested by the nonlinear stress-strain curves presented here. Our goal for the materially linear (isotropic and transversely isotropic) models was to generate an estimate of the modulus that was representative of in vivo conditions by forcing the linear model tangent to the measured curve at 15 mm Hg. While our method is only approximate, the fact that the linear modulus (0.57–1.01 N/mm^2) lies within the range of moduli calculated along the nonlinear stress-strain curve of Fig. 9 (0.27–1.32 N/mm^2) suggests that this method is reasonable.

One can also conclude from the identification results that the nonlinearity in the cornea's response to increasing pressure is due almost entirely to material nonlinearity rather than geometric nonlinearity. This conclusion is evident from Fig. 5, which shows that the model with geometric nonlinearity is almost identical to the fully linear model, yet when the modulus is allowed to vary, as in the materially nonlinear model of Fig. 6, the measured curve is approximated very closely. Furthermore, it appears that material nonlinearity may be important in modeling radial keratotomy. This is suggested to some extent by the fact that significantly more corneal curvature change was achieved with the nonlinear model than the linear ones. Further evidence is provided by the fact that the nonlinear modulus in the radial keratotomy model changed by as much as 80 percent from before the introduction of incisions to afterwards. In the pressurized but unincised mesh, the tangent modulus was different at points c and d (Fig. 9(*b*)) by almost a factor of five. Thus, the range of stresses due to membrane inflation alone is considerable. Of course, one would expect that the distribution of stresses would be different in a model that represented the relaxation of stresses along cut fibrils, and this might result in a larger or smaller range of stresses than was evident in the isotropic models considered here.

With only apical displacements available for identifying the properties, it was not possible to identify the five constants necessary to define a linear, transversely isotropic constitutive law. Instead, previous experimental results of Battaglioli and Kamm (1984) on human sclera were used to set the transverse modulus to $\frac{1}{10}$th the in-plane value; i.e., $n = 10$. In the same experiment, they also measured one of the Poisson's ratios for the sclera, finding that $\nu_{zx} \approx 0.5$.

To see how these measurements fit within the framework of linear transverse isotropy, a relationship among the parameters can be derived from the requirement that the material property matrix must be positive definite. For a matrix to be positive definite all its submatrices must have positive determinants. From (2), the requirement that the determinant of the first submatrix must be positive leads to the following equation:

$$1 - 2n\nu_{zx}^2(1 + \nu_{xy}) - \nu_{xy}^2 > 0 \qquad (8)$$

Assuming Battaglioli and Kamm's value of $\nu_{zx} = 0.5$, (8) can be written as

Downloaded From: https://biomechanical.asmedigitalcollection.asme.org on 06/28/2019 Terms of Use: http://www.asme.org/about-asme/terms-of-use

$$n < 2(1 - \nu_{xy}^2)/(1 + \nu_{xy}) \quad (9)$$

which implies that $n < 2$ for $\nu_{xy} > 0$. This contradicts their findings for human sclera, in which they concluded $n \geq 10$. If the cornea has a similar constitutive behavior to the sclera, as suggested by the similarity in their microstructures, then this implies that linear transverse isotropy is not an adequate representation of the cornea's anisotropy. However, that this does not demonstrate that a nonlinear, transversely isotropic model might not prove to be better suited to the cornea.

Odgen's model also proved to be inadequate to represent the measured corneal response. It should be noted that this form of hyperelasticity was chosen over the Mooney-Rivlin law because Odgen's law is more versatile. For example, a second-order Ogden's law contains the Mooney-Rivlin law as a special case. Models employing a two-parameter Mooney-Rivlin law that we subsequently analyzed confirmed this view, showing even less capacity for modeling the measured corneal response than Ogden's model. In view of the fact that many elastomers only begin to show increasing stiffness after 100 percent strain (see Han, 1992, for example), the failure of these hyperelastic models to adequately model the cornea's increasing stiffness, which climbs sharply after less than 10 percent strain, should not be surprising.

Of the models presented above, the materially nonlinear law captures the cornea's nonlinearity best. However, the fact that the materially nonlinear law works well for membrane inflation does not necessarily imply that it will work well for refractive surgery. Wray et al. (1994) compared a similar model to the clinical results of radial keratotomy reported in the Kansas City Study and in the University of Texas Study and found that it captures some clinical trends but not all. However, as they discuss, there are problems in comparing model results to the statistical results of clinical trials. For example, they compared the change in corneal curvature of their finite element model to the change in spherical equivalent of refraction reported from the clinical trials. Corneal curvature is a geometric property of the corneal surface, whereas refraction involves not only the corneal geometry but the eye's optics, retinal photoreceptor orientation, and even the cortical processing of the retinal image. Consequently, although the change in corneal curvature and the change in spherical equivalent of refraction typically follow the same trend, they are not necessarily the same in magnitude and in some cases can differ considerably. While this may not change their conclusions, it points out the difficulty in retrospectively comparing analytical models to clinical data. Another problem inherent in this sort of retrospective validation is apparent in the fact that the nearest time point available in the Kansas City Study was at three months, where contraction of the healing wounds would be expected to cause regression of the radial keratotomy effect. Thus, the acute effect being modeled is not necessarily represented in the clinical data. As noted by Wray et al. in their paper, the problem of comparing a "mean value eye" to the mean response of all eyes reported in a clinical study is also a concern.

As demonstrated by Pinsky and Datye (1991), the fibrillar microstructure of the cornea implies that considerable inhomogeneity in stiffness may result from incisions in the cornea. The relaxation in stress along the cut fibrils is not represented in an isotropic model and may account for some of the discrepancies between the results of Wray et al. and the clinical results they compare their model to. It is likely that a more sophisticated formulation that takes the cornea's unique lamellar arrangement into account, such as Pinsky and Datye's (1994), will be necessary to capture all the clinically significant effects. However, until controlled experimental and clinical tests of radial keratotomy and other refractive surgeries are performed with the specific intent of validating these models, it will not be possible to determine quantitatively how well any constitutive law or finite element formulation predicts the results of refractive surgery.

Other characteristics of the eye that may need to be considered to accurately model refractive surgery include the constitutive behavior of the sclera, the boundary conditions on the globe (e.g., the extraocular muscles), the effect (if any) of the internal structures of the eye (i.e., crystalline lens, ciliary processes, iris, choroid, retina), the inhomogeneity of the cornea and sclera, and the properties of the other layers of the cornea, such as Bowman's layer and Descemet's membrane.

In future studies, we will employ a computer-assisted videokeratographer, such as the Topographic Modeling System (Computed Anatomy, Inc, New York, NY), which optically scans the corneal topography and produces a three-dimensional map of the corneal surface. In previous studies, Bryant and Velinsky (1991) have shown that the output of this device can be used to construct a finite element mesh of the cornea that captures the corneal shape in considerable detail. This would not only eliminate the limitations of the geometric model assumed in the present study but might allow the material constants for a more sophisticated nonlinear anisotropic constitutive law to be identified by recording the corneal topography at different pressures. In fact, we propose that it may be possible to measure these material properties in vivo by using drugs that lower the intraocular pressure, such as beta blockers, in conjunction with corneal topographic measurements. This would enable biomechanical models of refractive surgery to be customized to each patient so that the surgical outcome could be more accurately predicted on an individual basis.

Acknowledgments

Supported in part by a grant from the Autry Foundation, Los Angeles, CA, by an unrestricted grant from Research to Prevent Blindness, Inc., New York, NY, and by grant EY10335 from the National Eye Institute, Bethesda, MD. Dr. McDonnell is a Research to Prevent Blindness William and Mary Greve International Research Scholar.

The authors gratefully acknowledge Don Ward of the Lions Doheny Eye Bank for the loan of the artificial anterior chamber, and Lori LaBree of the Doheny Eye Institute Biometry Core Module for assistance with statistical analyses.

References

Battaglioli, J. L., and Kamm, R. D., 1984, "Measurements of the Compressive Properties of Scleral Tissue," *Invest. Ophthalmol. Vis. Sci.*, Vol. 25, pp. 59–65.

Boresi, A. P., and Chong, K. P., 1987, *Elasticity in Engineering Mechanics*, Elsevier, New York, pp. 250–255.

Bryant, M. R., Velinsky, S. A., Plesha, M. E., and Clarke, G. P., 1987, "Computer-Aided Surgical Design in Refractive Keratotomy," *CLAO Journal*, Vol. 13, pp. 238–242.

Bryant, M. R., and Velinsky, S. A., 1991, "Design of Keratorefractive Surgical Procedures: Radial Keratotomy," ASME *Journal of Mechanical Design*, Vol. 113, pp. 150–157.

Chang, Sophia, Structural Research and Analysis Corp., personal communication, March 1994.

Cook, R. D., 1981, *Concepts and Applications of Finite Element Analysis*, 2nd ed., Wiley, New York.

COSMOS/M Advanced Modules User Guide, 1993, Part 1 (Volume 4), Version 1.70. Structural Research and Analysis Corporation, May.

Duffey, R. J., Tchah, H., and Lindstrom, R. L., 1989, "Human Cadaver Corneal Thinning for Experimental Refractive Surgery," *Refract. Corneal. Surg.*, Vol. 5, pp. 41–42.

Gill, P. E., Murray, W., and Wright, M. H., 1981, *Practical Optimization*, Academic Press, Orlando FL.

Han, P., ed., 1992, Tensile Testing, ASM International, Materials Park, OH, p. 142–143.

Hanna, K. D., Jouve, F., Bercovier, M. H., and Waring, G. O., 1988, "Computer Simulation of Lamellar Keratectomy and Laser Myopic Keratomileusis," *Refrac, Corneal Surg.*, Vol. 4, pp. 222–231.

Hanna, K. D., Jouve, F. E., Waring, G. O., and Ciarlet, P. G., 1989a, "Computer Simulation of Arcuate and Radial Incisions Involving the Corneoscleral Limbus," *Eye*, Vol. 3, pp. 227–239.

Hanna, K. D., Jouve, F. E., and Waring, G. O., 1989b, "Preliminary Computer Simulation of the Effects of Radial Keratotomy," *Arch. Ophthalmol.*, Vol. 107, pp. 911–918.

Hart, W. M., 1992, "Intraocular Pressure," *Adler's Physiology of the Eye*, Hart, W. M., ed., Mosby-Year Book, St. Louis, MO, pp. 263.

Downloaded From: https://biomechanical.asmedigitalcollection.asme.org on 06/28/2019 Terms of Use: http://www.asme.org/about-asme/terms-of-use

Hoeltzel, D. A., Altman, P., Buzard, K., and Choe, K., 1992, "Strip Extensiometry for Comparison of the Mechanical Response of Bovine, Rabbit, and Human Corneas," ASME JOURNAL OF BIOMECHANICAL ENGINEERING, Vol. 114, pp. 202–215.

Hjortdal, J. O., and Koch-Jensen, P., 1992, "In Situ Mechanical Behavior of the Human Cornea as Evaluated by Simultaneous Measurements of Corneal Strain, Corneal Surface Contour, and Corneal Thickness," *Invest. Ophthalmol. Vis. Sci.*, Vol. 33, pp. 895.

Huang, T., Bisarnsin, T., Schachar, R. A., and Black, T. D., 1988, "Corneal Curvature Change Due to Structural Alteration by Radial Keratotomy," ASME JOURNAL OF BIOMECHANICAL ENGINEERING, Vol. 110, pp. 249–253.

Jue, B., and Maurice, D. M., 1986, "The Mechanical Properties of the Rabbit and Human Cornea," *Journal of Biomechanics*, Vol. 19, pp. 847–853.

Pinsky, P. M., and Datye, D. V., 1991, "A Microstructurally-Based Finite Element Model of the Incised Human Cornea," *Journal of Biomechanics*, Vol. 24, pp. 907–922.

Pinsky, P. M., and Datye, D. V., 1994, "A Microstructurally-Based Mechanical Model of the Human Cornea With Application to Keratotomy," *Invest. Ophthalmol. Vis. Sci.*, Vol. 35(Suppl), pp. 1296.

Sjontoft, E., and Edmund, C., 1987, "In Vivo Determination of Young's Modulus of the Cornea," *Bulletin of Mathematical Biology*, Vol. 49, pp. 217–232.

Vito, R. P., Shin, T. J., and McCarey, B. E., 1989, "A Mechanical Model of the Cornea: The Effects of Physiological and Surgical Factors on Radial Keratotomy Surgery," *Refract. Corneal Surg.*, Vol. 5, pp. 82–88.

Waring, G. O., Lynn, M. J., Culbertson, W., Laibson, P. R., Lindstrom, R. D., McDonald, M. B., Myers, W. D., Obstrbaum, S. A., Rowsey, J. J., and Schanzlin, D. J., PERK Study Group, 1987, "Three-Year Results of the Prospective Evaluation of Radial Keratotomy (PERK) Study," *Ophthalmology*, Vol. 94, pp. 1339–1354.

Woo, S. L. Y., Kobayashi, A. S., Schlegel, and W. A., Lawrence, C., 1972, "Non-Linear Properties of Intact Cornea and Sclera," *Exp. Eye Res.*, Vol. 14, pp. 29–39.

Wray, W. O., Best, E. D., and Cheng, L. Y., 1994, "A Mechanical Model for Radial Keratotomy: Towards a Predictive Capability," ASME JOURNAL OF BIOMECHANICAL ENGINEERING, Vol. 116, pp. 56–61.

Downloaded From: https://biomechanical.asmedigitalcollection.asme.org on 06/28/2019 Terms of Use: http://www.asme.org/about-asme/terms-of-use